^{159}Dy Electron-Capture: A New Candidate for Neutrino Mass Determination

Z. Ge,[1,*] T. Eronen,[1,†] K. S. Tyrin,[2] J. Kotila,[3,4] J. Kostensalo,[1] D. A. Nesterenko,[1] O. Beliuskina,[1]
R. de Groote,[1] A. de Roubin,[5] S. Geldhof,[1,§] W. Gins,[1] M. Hukkanen,[1,5] A. Jokinen,[1] A. Kankainen,[1]
Á. Koszorús,[6] M. I. Krivoruchenko,[2,8,‡] S. Kujanpää,[1] I. D. Moore,[1] A. Raggio,[1] S. Rinta-Antila,[1] J. Suhonen,[1]
V. Virtanen,[1] A. P. Weaver,[8] and A. Zadvornaya[1]

[1]*Department of Physics, University of Jyväskylä, P.O. Box 35, FI-40014 Jyväskylä, Finland*
[2]*National Research Centre "Kurchatov Institute," Ploschad' Akademika Kurchatova 1, 123182 Moscow, Russia*
[3]*Finnish Institute for Educational Research, University of Jyväskylä, P.O. Box 35, FI-40014 Jyväskylä, Finland*
[4]*Center for Theoretical Physics, Sloane Physics Laboratory Yale University, New Haven, Connecticut 06520-8120, USA*
[5]*Centre d'Etudes Nucléaires de Bordeaux Gradignan, UMR 5797 CNRS/IN2P3—Université de Bordeaux,*
19 Chemin du Solarium, CS 10120, F-33175 Gradignan Cedex, France
[6]*Department of Physics, University of Liverpool, Liverpool L69 7ZE, United Kingdom*
[7]*Institute for Theoretical and Experimental Physics, NRC "Kurchatov Institute,"*
B. Cheremushkinskaya 25, 117218 Moscow, Russia
[8]*School of Computing, Engineering and Mathematics, University of Brighton, Brighton BN2 4JG, United Kingdom*

The ground state to ground state electron-capture Q value of ^{159}Dy ($3/2^-$) has been measured directly using the double Penning trap mass spectrometer JYFLTRAP. A value of 364.73(19) keV was obtained from a measurement of the cyclotron frequency ratio of the decay parent ^{159}Dy and the decay daughter ^{159}Tb ions using the novel phase-imaging ion-cyclotron resonance technique. The Q values for allowed Gamow-Teller transition to $5/2^-$ and the third-forbidden unique transition to $11/2^+$ state with excitation energies of 363.5449(14) keV and 362.050(40) keV in ^{159}Tb were determined to be 1.18(19) keV and 2.68(19) keV, respectively. The high-precision Q value of transition $3/2^- \rightarrow 5/2^-$ from this work, revealing itself as the lowest electron-capture Q value, is used to unambiguously characterize all the possible lines that are present in its electron-capture spectrum. We performed atomic many-body calculations for both transitions to determine electron-capture probabilities from various atomic orbitals and found an order of magnitude enhancement in the event rates near the end point of energy spectrum in the transition to the $5/2^-$ nuclear excited state, which can become very interesting once the experimental challenges of identifying decays into excited states are overcome. The transition to the $11/2^+$ state is strongly suppressed and found unsuitable for measuring the neutrino mass. These results show that the electron-capture in the ^{159}Dy atom, going to the $5/2^-$ state of the ^{159}Tb nucleus, is a new candidate that may open the way to determine the electron-neutrino mass in the sub-eV region by studying electron-capture. Further experimental feasibility studies, including coincidence measurements with realistic detectors, will be of great interest.

The neutrino is perhaps the most mysterious particle of all elementary particles. The problem of the overall scale of neutrino masses is a matter of paramount importance in the search for generalizations of the standard model, as well as for cosmology. Numerous modern experiments on neutrino oscillations [1–3] allow extracting nonzero differences between the neutrino masses squared and also the oscillation parameters. These experiments are insensitive to the overall scale of neutrino masses. However, they limit the effective mass of electron antineutrinos to be at least 0.048 eV/c^2 and 0.0085 eV/c^2 for the inverted and normal mass orderings, respectively [3]. Indirect measurements of the neutrino mass, which also allow to clarify the Dirac or Majorana nature of neutrinos, are conducted in the

search of neutrinoless double-β^- decay with a sensitivity of about 0.1 eV/c^2 [4–7] and neutrinoless double-electron capture [8]. The only direct and model-independent methods for measuring the mass of neutrinos are based on the study of single electron-capture (EC) [9], while the mass of antineutrinos is measured in single-β^- decays [10].

Presently, the most stringent upper limit of 0.8 eV/c^2 (90% confidence level) for the effective electron antineutrino mass $m_{\bar{\nu}_e}$ originates from very recent data obtained with the KATRIN (KArlsruhe TRitium Neutrino) experiment via investigation of the emitted electron spectrum endpoint of tritium β^- decay [10]. The most stringent upper limit of the effective electron-neutrino mass m_{ν_e} is as large as 150 eV/c^2 [11] (95% confidence level), derived from

the analysis of the EC endpoint of ^{163}Ho, which is being used for next-generation direct neutrino-mass determination experiments such as ECHo [9] and HOLMES [12].

The search for potential isotopes for possible future long-term and high-sensitivity (anti)neutrino-mass determination experiments [7,13–16] in the pursuit of sub-eV sensitivity, is of great interest. For β^- decay spectra, the neutrino-mass sensitivity depends on the fraction of events close to the end point, where the cumulative decay rate is proportional to the phase-space factor and scales with Q^{-3}. For EC, the event rate dependency on Q value near the endpoint is more sensitive and depends on how close the decay Q value is to the ionization energy of the captured electron. For EC, the cumulative event rate near the end point is proportional to Q^{-2}, and it increases when the electron orbitals have an ionization energy close to the value of Q. Nuclides, favored for such direct neutrino-mass experiments, are the ones with a small Q and the electron orbitals close to the threshold. ^{159}Dy, studied here, decays only by EC and its ground state to ground state Q value (Q_{EC}^{gs}) 365.2(12) keV [17,18] is close to the excitation energies (E_i^*) [19] of two candidate excited states having spin parity $5/2^-$ and $11/2^+$ in the daughter nucleus ^{159}Tb; see Table I. The EC Q values to the excited states are expected to be very small. Especially EC to the $5/2^-$ state is of significant interest since it is of Gamow-Teller type and has been experimentally confirmed to exist with a branching ratio $1.9(5) \times 10^{-6}$ [20]. Branching ratio of EC to the $11/2^+$ state is tiny compared to $5/2^-$ state, and this decay branch has not been observed. The total energy of the neutrino emitted in EC decay is determined by the atomic binding energies of the possible allowed atomic shells of the captured electron. In the present case, captures of electrons occupying the K and L shells for the transition ^{159}Dy$(3/2^-) \rightarrow ^{159}Tb^*(5/2^-)$ are energetically forbidden. Only electrons from s and $p_{1/2}$ levels from the third and higher shells (M1, M2, N1, N2, O1, O2, and P1) can

possibly be captured due to angular momentum conservation and the finite overlap of their wave function with the nucleus. This makes the EC energy even smaller, as tabulated in Table I. The nuclear excitation energies of the two daughter states are already rather accurately known (< 40 eV). The main uncertainty in the Q value is due to the 1.2 keV uncertainty in the ground state to ground state Q value, which is primarily determined from ^{159}Dy(EC)^{159}Tb decay data [17,19,20]. With this large uncertainty it is impossible to model the EC spectrum shape, especially near the end point where the decay rate is extremely sensitive to the Q value. The current precision does not even allow an order-of-magnitude scale estimate.

In this Letter, we report on the first direct ^{159}Dy ground state to ground state EC Q-value determination. Based on the results, we performed atomic many-body calculations in order to determine the partial EC rates from different atomic shells for the two discussed EC transitions: the allowed Gamow-Teller transition $3/2^- \rightarrow 5/2^-$ and the third-forbidden unique transition $3/2^- \rightarrow 11/2^+$. We have also determined the partial half-lives of the captures from different atomic shells for the Gamow-Teller transition by normalizing to the measured total EC branching to the $5/2^-$ state.

The measurements were conducted at the Ion Guide Isotope Separator On-Line facility (IGISOL) using the double Penning trap mass spectrometer JYFLTRAP [22] in the accelerator laboratory of the University of Jyväskylä, Finland [23]. To produce ^{159}Dy$^+$ ions, a proton beam of 40 MeV in energy from the K-130 cyclotron was used to bombard a dysprosium target with natural abundance. Ions of stable daughter ^{159}Tb$^+$ were separately produced with an offline glow-discharge ion source.

The phase-imaging ion-cyclotron resonance technique [24,25] was used to measure the cyclotron frequencies $\nu_c = (1/2\pi)(q/m)B$, where q/m is the charge-to-mass ratio of the measured ^{159}Dy$^+$ and ^{159}Tb$^+$ ions and B the

TABLE I. Q values of the EC transitions from the $3/2^-$ ground state (gs) of the parent nucleus ^{159}Dy to the potential low Q-value excited states of the daughter nucleus ^{159}Tb. The first column indicates the excited final state of interest for the low Q-value transition or the ground state with spin parities indicated. The second column gives the decay type. The third column lists the experimental excitation energy E_i^* with the experimental error [19] and the fourth column gives the derived experimental decay Q_{EC}^i ($i = 1, 2$) value. The fifth to ninth columns denoted as Δ_x^i give the distance of the Q_{EC}^i value to the binding energy ε_x (from [21]) of the electrons in the daughter atoms. The last column indicates the source of values on each row, either from atomic mass evaluation literature (AME2020) [17,18] or obtained from this work. The decay Q values and excitation energies are in units of keV.

Final state	Decay type	E_i^*	Q_{EC}^i	Δ_{M1}^i	Δ_{M2}^i	Δ_{N1}^i	Δ_{N2}^i	Δ_{O1}^i	Source
$5/2^-$	Allowed	363.5449(14)	1.7(12)	−0.3(12)	−0.1(12)	1.3(12)	1.3(12)	1.6(12)	AME2020
			1.18(19)	−0.78(19)	−0.58(19)	0.79(19)	0.87(19)	1.14(19)	This work
$11/2^+$	3rd forbidden unique	362.050(40)	3.2(12)	1.2(12)	1.4(12)	2.8(12)	2.8(12)	3.1(12)	AME2020
			2.68(19)	0.63(19)	0.84(19)	2.26(19)	2.35(19)	2.62(19)	This work
$3/2^+$		0	365.2(12)						AME2020
			364.73(19)						This work

magnetic field. We used the scheme that allows direct determination of ν_c via the sideband coupling frequency $\nu_c = \nu_+ + \nu_-$, where ν_+ is the trap-modified cyclotron frequency and ν_- the magnetron frequency. Phase accumulation time $t = 514$ ms was chosen for both $^{159}\text{Dy}^+$ and $^{159}\text{Tb}^+$ ions to ensure that the spot of interest was resolved from any leaked isobaric, isomeric, and molecular contamination. No contaminating ions were observed.

The parent ^{159}Dy and daughter ^{159}Tb ion cyclotron frequency measurements were interleaved by changing between the two every 3 minutes to minimize the uncertainty contribution of the magnetic field fluctuation in the measured cyclotron frequency ratio. The data was analyzed by dividing the collected data into approximately 12 minute sections in order to have a reasonable amount of statistics for fitting the magnetron and cyclotron phase spots using the maximum likelihood method. Ion bunches up to 5 detected ions were used in the analysis. Additionally, a count-rate class analysis [26], in which the frequency data were split up by the number of ions simultaneously present in the precision trap, was carried out. No evidence of a correlation between frequency measurements and count rate was observed, which indicated no systematic frequency shifts at the achieved statistical precision level due to ion-ion interactions. Furthermore, ^{159}Dy and ^{159}Tb ions being mass doublets cancel many of the systematic uncertainties in the cyclotron frequency ratio [27].

The $Q_{\text{EC}}^{\text{gs}}$ is obtained from the mass difference of ^{159}Dy and ^{159}Tb using the mass-energy equivalence formula $E = mc^2$:

$$Q_{\text{EC}} = (M_i - M_f)c^2 = (R-1)(M_f - m_e)c^2 + \Delta B_{\text{if}}, \quad (1)$$

where M_i and M_f are the atomic masses of the parent and daughter atoms, respectively, and $R = \nu_{c,f}/\nu_{c,i}$ is their cyclotron frequency ratio obtained in charge state 1+. The value ΔB_{if} describes the contribution from electron binding energy differences of the parent and daughter atoms (here, 0.075 25(60) eV for $^{159}\text{Dy}^+$ and $^{159}\text{Tb}^+$ [28]). m_e is the mass of electron. Three sets of data were collected (see Fig. 1). The normalized χ^2 for the sets were 1.2, 0.9, and 1.0. The uncertainty of the first was expanded with the square root of it, marginally affecting the final weighted mean ratio $\bar{R}$. The final weighted mean frequency ratio $\bar{R}$ is 1.000 002 463 8 (13), which results in $Q_{\text{EC}}^{\text{gs}} = 364.73(19)$ keV.

The obtained $Q_{\text{EC}}^{\text{gs}}$ from this work is more than 6 times more precise and 0.47 keV smaller than the AME2020 value, which was derived primarily from an EC decay measurement of $^{159}\text{Dy}(\text{EC})^{159}\text{Tb}$ [17]. The newly measured high-precision $Q_{\text{EC}}^{\text{gs}}$, together with the accurate nuclear energy level data, yields Q_{EC}^i values of 1.18(19) keV and 2.68(19) keV for the $5/2^-$ and $11/2^+$ states in ^{159}Tb, respectively. Q values of different atomic electron shell captures are tabulated in Table I. Which orbital
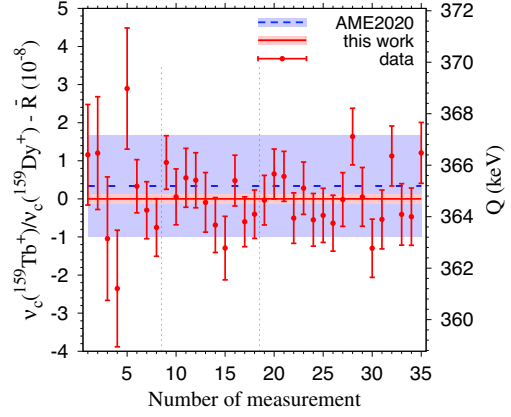

FIG. 1. Comparison of results obtained in this work and the literature value (AME2020) [17,18]. In total, 36 individual frequency ratios were measured in three time slots.

electrons take part in the EC process and the absolute Q values of the decays are crucial for modeling the spectrum shape near the end point. In this work, M2 capture to the $5/2^-$ state is confirmed to be energetically forbidden at 3.3σ level, revealing N1 to be the first energetically possible capture at 4.0σ level. In addition, the M1 capture to the $11/2^+$ state is confirmed to be positive at 3.7σ level and captures can proceed from M1 and higher orbits. The unambiguous characterization of all the possible lines in the EC spectrum at a significance level of at least 3σ for the transitions makes the modeling of their shape possible.

To estimate the EC partial half-lives and the distribution of energy released in the decays, we have performed Dirac-Hartree-Fock atomic many-body calculations. The EC capture rate is determined by the standard β-decay Hamiltonian. The probability depends on the wave function of the electrons inside the nucleus and on the exchange-and-overlap factor of the spectator electrons due to the nonorthogonality of the atomic shells of the parent and daughter atoms, as well as the nuclear matrix element.

The energy distribution of EC events is represented as the incoherent sum of the contributions of individual orbitals:

$$\rho(E) = \frac{G_\beta^2}{(2\pi)^2} \sum_x n_x \mathcal{B}_x \beta_x^2 C_x p_\nu(E_\nu) E_\nu \frac{\Gamma_x/(2\pi)}{(E - \varepsilon_x)^2 + \Gamma_x^2/4}, \quad (2)$$

where $E = Q_{\text{EC}}^i - E_\nu$, Q_{EC}^i is the Q value of the decay, E_ν is the neutrino energy, $\lambda(E)$ is the total decay probability in the interval $(E, Q_{\text{EC}}^i - m_\nu)$; $G_\beta = G_F \cos\theta_C$, where G_F is the Fermi constant and θ_C is the Cabibbo angle; $p_\nu(E_\nu) = \sqrt{E_\nu^2 - m_\nu^2}$ is the neutrino momentum, ε_x is the energy of the electron hole with quantum numbers $x = (n, l, j)$ of the daughter atom, and n_x is the occupation fraction of electrons in a partially filled shell x of the parent atom

($n_x = 1$ for closed shells). The shape factor C_x contains the nuclear-structure information in terms of nuclear form factors [29]. Γ_x is the intrinsic linewidth of the Breit-Wigner resonance centered at the energies ε_x. The amplitudes β_x, which characterize the electron wave functions inside the nucleus, and the exchange-and-overlap factors $\mathcal{B}_x$ are given for a broad set of atomic numbers and orbitals, e.g., in [30] and here calculated for all orbitals of ^{159}Dy and ^{159}Tb* atoms by using the atomic structure software package GRASP2018 [31]. The nuclear charge density is given by the Fermi distribution with the root mean square radius of $R_{\mathrm{nucl.}} = 5.1$ fm and thickness 2.3 fm. The parent ^{159}Dy atom is in the ground state, while the daughter atom ^{159}Tb* is described by the electron wave functions depending on the hole x. Electrons of the daughter atom inherit quantum numbers from the configuration $[\mathrm{Xe}](4f)^{10}(6s)^2$ of the parent ^{159}Dy atom. The exchange-and-overlap factors $\mathcal{B}_x$ calculated in the Vatai approach [30] deviate from unity by 25% or less.

The total decay constant $\lambda \equiv \lambda(Q_{\mathrm{EC}}^i - m_\nu)$ is calculated from

$$\lambda(E) = \int_0^E \rho(E')dE'. \tag{3}$$

In the narrow-width approximation $\lambda \approx \sum_x \lambda_x$, the partial decay constants equal

$$\lambda_x = \frac{G_\beta^2}{(2\pi)^2} n_x \mathcal{B}_x \beta_x^2 C_x p_\nu (Q_{\mathrm{EC}}^i - \varepsilon_x)(Q_{\mathrm{EC}}^i - \varepsilon_x). \tag{4}$$

For the presently discussed transitions to the $5/2^-$ state and $11/2^+$ state, the shape factor contains only one nuclear form factor in the leading order.

For the EC to the $5/2^-$ state, the shape factor can be written as $C_x = [^A F_{101}^{(0)}]^2$, with the nuclear form factor given in terms of the Gamow-Teller nuclear matrix element as

$$^A F_{101}^{(0)} = -\frac{g_A}{\sqrt{2J_i + 1}} M_{\mathrm{GT}}. \tag{5}$$

Here. g_A is the strength of the weak axial coupling, J_i the angular momentum of the initial state, and M_{GT} the Gamow-Teller nuclear matrix element [32]. In fact, for this decay transition we do not need the value of the form factor $^A F_{101}^{(0)}$ since we normalize λ by the available half-life for the Gamow-Teller transition, derived from the measured branching [20] and the total half-life [19]. For this transition, the experimental binding energies and normalized partial half-lives are listed in Table II.

The summation in Eq. (2) runs over the electron orbitals shown in Table II, as well as over the M1 and M2 orbitals. Although M1 and M2 are outside the kinematically accessible energy region, the tails of their Breit-Wigner

TABLE II. Normalized partial half-lives for the Gamow-Teller EC transition $3/2^- \to 5/2^-$. The first line lists the atomic orbitals x with a positive EC Q value; the second line shows the corresponding electron binding energies of the daughter ^{159}Tb* atom [21]. The last line lists the resulting partial EC half-lives after normalizing to the total half-life 2.08×10^5 years of the Gamow-Teller transition from [20]. The level P1 is calculated using the GRASP2018 software package [31] for an isolated atom of ^{159}Tb* in the configuration $[\mathrm{Xe}](4f)^{10}(6s)^1$.

x	N1	N2	O1	O2	P1
ε_x [eV]	396	322.4	45.6	28.7	9.5
$t_{1/2}$ [year]	3.0×10^5	5.8×10^6	8.9×10^5	2.6×10^7	1.3×10^7

amplitudes have a significant effect on the number of events for $E \lesssim Q_{\mathrm{EC}}^i$. The electromagnetic decay widths Γ_x of the N1, N2, M1, and M2 electron holes in ^{159}Tb* atom are taken from Ref. [33]; the data for $x = $ O1, O2, P1 are not available, so we assume $\Gamma_{\mathrm{O1,O2,P1}} = \Gamma_{\mathrm{N2}} = 5.26$ eV. The widths of the levels N1, N2, M1, and M2 closest to the threshold are known with an accuracy of 10%, 10%–15%, 5%, and 5%–10%, respectively [33]. The corresponding uncertainties in the spectrum do not exceed 30%, while the integral over the spectrum is almost independent of the level widths. The experimental error in Q_{EC}^i introduces through the phase-space volume about 50% uncertainty in the half-life estimates.

The computed calorimetric ^{163}Ho spectrum of Fig. 2 takes the electron orbitals M1, M2, N1, N2, O1, and O2 into account with the parameters given in Ref. [9]. The distances from the end point to the nearest peak for dysprosium (N1) and holmium (M2) are almost the same. Proximity of the M1 and M2 orbitals of dysprosium to the end point partly compensates the difference between the absolute EC rates of dysprosium and holmium at $E \lesssim Q_{\mathrm{EC}}^i$. The normalized cumulative distribution of the EC events near the end point equals $[\lambda - \lambda(E)]/\lambda \approx C_\nu p_\nu^3(E_\nu)$, where $C_\nu = 0.0061/\mathrm{keV}^3$ for dysprosium and $0.00056/\mathrm{keV}^3$ for holmium. The M1 and M2 orbitals increase the number of events in the end-point region by an order of magnitude. The same absolute numbers of events near the end point are provided by the ratio between the numbers of dysprosium atoms decaying to Tb$^*(5/2^-)$ and holmium atoms: $R(^{159}\mathrm{Dy}/^{163}\mathrm{Ho}) = T_{1/2}[^{159}\mathrm{Dy} \to {}^{159}\mathrm{Tb}^*(5/2^-)]/T_{1/2}(^{163}\mathrm{Ho})C_\nu(^{163}\mathrm{Ho})/C_\nu(^{159}\mathrm{Dy}) = 4.2$, while the total numbers of atoms before the filtering are in the ratio $R_0(^{159}\mathrm{Dy}/^{163}\mathrm{Ho}) = 4.2/1.9 \times 10^{-6} = 2.2 \times 10^6$. The smallness of C_ν values limits, due to statistical requirements, the sensitivity of EC experiments measuring the mass of electron neutrino. To improve sensitivity, reliable parameterization of the energy spectrum away from peaks is also necessary, taking into account the dependence of the
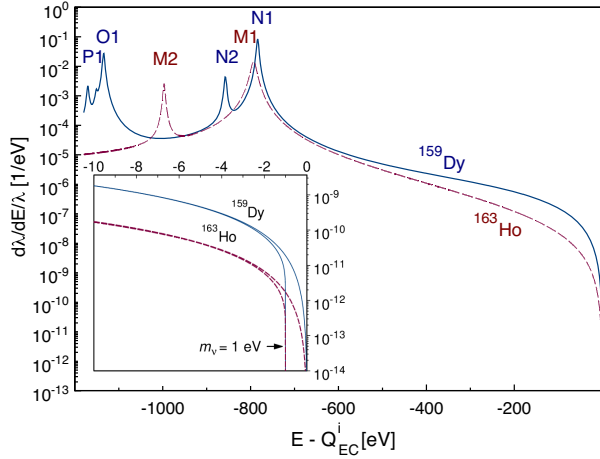
FIG. 2. The solid curve describes the normalized distribution over the released energy of EC events in the ^{159}Dy atom with the transition to the ^{159}Tb atom having a nucleus in the $5/2^-$ excited state. N1, N2, O1, and P1 indicate electron holes of the ^{159}Tb atom; the O2 hole is barely discernible and not labeled. The dashed curve shows the normalized distribution in energy of the ^{163}Ho EC events. M1 and M2 are electron holes of the ^{163}Dy atom. The energy E released in the electron capture takes values over the entire kinematically allowed region of the ^{159}Dy decay. Q_{EC}^i is the difference in energy of the parent and daughter atoms. A larger fraction of events lands near the end point for ^{159}Dy than for ^{163}Ho. The inset in the lower left part of the figure shows on an enlarged scale the energy spectra of dysprosium and holmium close to the threshold value to illustrate the effect of the neutrino masses of 1 and 0 eV/c^2.

electron level widths and decay constants on energy. Decays accompanied by shakeup and shakeoff excitations with the associated formation of multiple holes in the electron shell generate a fine structure of the spectrum [34–39], which is experimentally visible in holmium EC and is described well theoretically [40,41].

The decay to the $11/2^+$ state gathers contributions from the M1–M5, N1–N7, O1–O3, and P1 atomic orbitals. The decay rate involves one nuclear form factor that we have computed using the microscopic interacting boson-fermion model (IBFM-2). In this manner, we obtain an estimate of the half-life of $t_{1/2} \sim 10^{25}$ years for this transition, thus excluding it as a candidate for electron-neutrino mass measurements. There is also no experimental evidence for the existence of this transition.

The transition to the $5/2^-$ state has an experimentally measured half-life of 2.08×10^5 years [20]. This measured half-life can be used, together with the computed partial decay constants λ_x, to determine the normalized partial half-lives of the dominant EC channels. Using the computed decay constants and the IBFM-2 computed nuclear matrix element, one obtains a theoretical half-life that is consistent with the measured one. Figure 2 shows the calculated EC spectrum. For comparison, the spectrum is also given for ^{163}Ho. Both spectra are normalized to unity. It is clear that a larger fraction of events lands near the end point for ^{159}Dy than for ^{163}Ho. This is mostly due to M1 and M2 orbitals, which, although energetically forbidden (see Table I) for EC with ^{159}Dy, affect the distribution due to the low energy tails of the M1 and M2 resonances in the end-point region.

In conclusion, our findings reveal that the Q_{EC} of 1.18(19) keV for the transition ^{159}Dy$(3/2^-) \rightarrow$ ^{159}Tb$^*(5/2^-)$ is lower than the ground state to ground state Q_{EC} of ^{163}Ho, which is used in presently running or planned direct neutrino-mass experiments. Therefore, this allowed transition, with a universal spectral shape driven by a single decay matrix element and known branching ratio, becomes a potential candidate for effective electron neutrino-mass measurements. Proximity of Q_{EC} and atomic lines N1, M1, and M2 with values of 0.79(19) keV, $-0.78(19)$ keV, and -0.58(19) keV, respectively, indicates a significant potential of this EC transition for a self-calibrated and high-sensitivity EC experiment in the direct neutrino-mass determination. The background from the EC to other states of ^{159}Tb can be suppressed by coincident registration of de-excitation gamma rays from the $5/2^-$ state of the nucleus. Such event selection is used in the search for neutrinoless double electron-capture accompanied by nuclear excitations [8]. Decay to the $5/2^-$ level has a branching ratio of only 1.9×10^{-6}. In order to achieve sub-eV sensitivity, the measurement of the neutrino mass requires reliable coincidence measurements between the calorimeter and the γ detector to identify only a very small fraction of total events, as well as a low background and a high counting rate of microcalorimeters.

We also want to point out that the Gamow-Teller EC transition to the $5/2^-$ state also serves as one of the most prospective transitions for a possible relic antineutrino capture experiment [42]. Here, the very small Q value, reported in this Letter, implies a promisingly high sensitivity to relic neutrinos requiring orders of magnitude less active material than needed for other suggested candidate nuclei like ^{163}Ho or ^{157}Tb.

*Corresponding author.
zhuang.z.ge@jyu.fi
†Corresponding author.
tommi.eronen@jyu.fi
‡Corresponding author.
mikhail.krivoruchenko@itep.ru
§Present address: KU Leuven, Instituut voor Kern- en Stralingsfysica, B-3001 Leuven, Belgium.

[1] Y. Fukuda *et al.*, Phys. Rev. Lett. **81**, 1562 (1998).
[2] S. Bilenky, *Introduction to the Physics of Massive and Mixed Neutrinos*, 2nd ed., Lecture Notes in Physics Vol. 947 (Springer-Verlag, Berlin Heidelberg, 2018).
[3] P. A. Zyla *et al.* (Particle Data Group), Prog. Theor. Exp. Phys. (**2020**), 083C01.
[4] J. Suhonen and O. Civitarese, Phys. Rep. **300**, 123 (1998).
[5] F. T. Avignone, S. R. Elliott, and J. Engel, Rev. Mod. Phys. **80**, 481 (2008).
[6] J. D. Vergados, H. Ejiri, and F. Šimkovic, Rep. Prog. Phys. **75**, 106301 (2012).
[7] H. Ejiri, J. Suhonen, and K. Zuber, Phys. Rep. **797**, 1 (2019).
[8] K. Blaum, S. Eliseev, F. A. Danevich, V. I. Tretyak, S. Kovalenko, M. I. Krivoruchenko, Y. N. Novikov, and J. Suhonen, Rev. Mod. Phys. **92**, 045007 (2020).
[9] L. Gastaldo *et al.*, Eur. Phys. J. Special Topics **226**, 1623 (2017).
[10] M. Aker *et al.*, arXiv:2105.08533.
[11] C. Velte *et al.*, Eur. Phys. J. C **79**, 1026 (2019).
[12] M. Faverzani *et al.*, J. Low Temp. Phys. **184**, 922 (2016).
[13] M. T. Mustonen and J. Suhonen, J. Phys. G **37**, 064008 (2010).
[14] J. Suhonen, Phys. Scr. **89**, 054032 (2014).
[15] A. De Roubin, J. Kostensalo, T. Eronen, L. Canete, R. P. De Groote, A. Jokinen, A. Kankainen, D. A. Nesterenko, I. D. Moore, S. Rinta-Antila, J. Suhonen, and M. Vilén, Phys. Rev. Lett. **124**, 222503 (2020).
[16] Z. Ge *et al.*, Phys. Rev. C **103**, 065502 (2021).
[17] W. Huang, M. Wang, F. Kondev, G. Audi, and S. Naimi, Chin. Phys. C **45**, 030002 (2021).
[18] M. Wang, W. Huang, F. Kondev, G. Audi, and S. Naimi, Chin. Phys. C **45**, 030003 (2021).
[19] National Nuclear Data Center, available at https://www.nndc.bnl.gov/ (2020/4/7) (2021).
[20] B. Myslek, Z. Sujkowski, and B. Kotlinska, *Proceedings of the Conference on the Electron Capture and Higher Order Processes in Nuclear Decays, Debrecen, Hungary, 1968*, edited by D. Berenyi (Eoetvoe, Budapest, 1969), Vol. 1, pp. 102–7.
[21] X-ray data booklet, available at https://xdb.lbl.gov (2021/05/01) (2021).
[22] T. Eronen and J. C. Hardy, Eur. Phys. J. A **48**, 1 (2012).
[23] I. D. Moore, T. Eronen, D. Gorelov, J. Hakala, A. Jokinen, A. Kankainen, V. S. Kolhinen, J. Koponen, H. Penttilä, I. Pohjalainen, M. Reponen, J. Rissanen, A. Saastamoinen, S. Rinta-Antila, V. Sonnenschein, and J. Äystö, Nucl. Instrum. Methods Phys. Res., Sect. B **317**, 208 (2013).
[24] S. Eliseev, K. Blaum, M. Block, A. Dörr, C. Droese, T. Eronen, M. Goncharov, M. Höcker, J. Ketter, E. M. Ramirez, D. A. Nesterenko, Y. N. Novikov, and L. Schweikhard, Appl. Phys. B **114**, 107 (2014).
[25] D. A. Nesterenko, T. Eronen, A. Kankainen, L. Canete, A. Jokinen, I. D. Moore, H. Penttilä, S. Rinta-Antila, A. de Roubin, and M. Vilen, Eur. Phys. J. A **54**, 154 (2018).
[26] A. Kellerbauer, K. Blaum, G. Bollen, F. Herfurth, H. J. Kluge, M. Kuckein, E. Sauvan, C. Scheidenberger, and L. Schweikhard, Eur. Phys. J. D **22**, 53 (2003).
[27] C. Roux, K. Blaum, M. Block, C. Droese, S. Eliseev, M. Goncharov, F. Herfurth, E. M. Ramirez, D. A. Nesterenko, Y. N. Novikov, and L. Schweikhard, Eur. Phys. J. D **67**, 146 (2013).
[28] A. Kramida, Yu. Ralchenko, J. Reader, and NIST ASD Team, NIST Atomic Spectra Database (ver. 5.8), [Online]. Available: https://physics.nist.gov/asd [2021, January 19]. National Institute of Standards and Technology, Gaithersburg, MD. (2020).
[29] H. Behrens and W. Bühring, *Electron Radial Wave Functions and Nuclear Beta-decay (International Series of Monographs on Physics)* (Clarendon Press, Oxford, 1982).
[30] W. Bambynek, H. Behrens, M. H. Chen, B. Crasemann, M. L. Fitzpatrick, K. W. D. Ledingham, H. Genz, M. Mutterer, and R. L. Intemann, Rev. Mod. Phys. **49**, 77 (1977).
[31] C. Froese Fischer, G. Gaigalas, P. Jönsson, and J. Bieroń, Comput. Phys. Commun. **237**, 184 (2019).
[32] J. Suhonen, *From Nucleons to Nucleus* (Springer–Verlag Berlin Heidelberg, Springer, Gaithersburg MD, 20899, 2007).
[33] J. Campbell and T. Papp, At. Data Nucl. Data Tables **77**, 1 (2001).
[34] R. G. H. Robertson, Phys. Rev. C **91**, 035504 (2015).
[35] A. Faessler, C. Enss, L. Gastaldo, and F. Šimkovic, Phys. Rev. C **91**, 064302 (2015).
[36] A. Faessler and F. Šimkovic, Phys. Rev. C **91**, 045505 (2015).
[37] A. Faessler, L. Gastaldo, and F. Šimkovic, J. Phys. G **42**, 015108 (2015).
[38] A. Faessler, L. Gastaldo, and F. Šimkovic, Phys. Rev. C **95**, 045502 (2017).
[39] A. De Rújula and M. Lusignoli, J. High Energy Phys. 05 (2016) 015.
[40] M. Braß, C. Enss, L. Gastaldo, R. J. Green, and M. W. Haverkort, Phys. Rev. C **97**, 054620 (2018).
[41] M. Braß and M. W. Haverkort, New J. Phys. **22**, 093018 (2020).
[42] J.-Y. Lee, Y. Kim, and S. Chiba, arXiv:1811.05183.